ELSEVIER

Journal of Nuclear Materials 283–287 (2000) 637–641

journal of nuclear materials

www.elsevier.nl/locate/jnucmat

A physically based constitutive model for a V–4Cr–4Ti alloy

E.G. Donahue *, G.R. Odette, G.E. Lucas

Department of Mechanical and Environmental Engineering, University of California, Santa Barbara, CA 93106, USA

Abstract

A constitutive model for low-to-intermediate temperatures, strains, and strain rates is developed for the program heat of V–4Cr–4Ti. The basic form of the model is derived from more general dislocation-based models of yield stress and strain hardening. The physically based forms are fit to a database derived from tensile tests carried out over a wide range of temperatures and strain rates. Yield and post-yield strain-hardening contributions to the flow stress are additive. The yield stress has both thermally activated and athermal components. The former is described by a two-mechanism activated dislocation slip model, with contributions that appear to arise from both lattice friction (at lower temperatures) and dislocation pinning by interstitial impurities (at higher temperatures). The yield stress data can be correlated using a strain rate-compensated temperature. The model uses a temperature-weighted average of the two mechanisms. Post-yield strain hardening was found to be approximately athermal. Strain hardening is fit to a two-component modified Voce-type saturating flow stress model. The constitutive model is also used to determine the flow stability limits as estimates of uniform tensile strains. The relatively compact, but mechanism-based, semi-empirical model has a number of both fundamental and practical advantages that are briefly outlined.

1. Introduction

It is axiomatic that 21st century fusion technology will employ sophisticated design and structural assessment tools that require a complete, accurate and well-understood characterization of the mechanical behavior of the constituent structural materials. The basic stress–strain, or constitutive laws, are one of several key parts of the requisite property database, and are the focus of this paper. In the simplest case of current code compliance assessments, the constitutive database might be comprised simply of tabulations of strength and so-called ductility 'properties' derived from standard tensile tests. However, standard engineering tensile properties, involving ill-defined measures of ductility, are insufficient to support more rigorous finite element method (FEM) simulations of the detailed behavior of complex structural configurations.

Constitutive properties are also required to measure, apply and obtain a basic understanding of the long list of life-limiting failure-related properties and parameters, such as fracture toughness. The property database must also characterize the multiple in-service changes that are controlled by combinations of a very large number of environmental and as-fabricated material variables. Creation of such information is enormously time consuming and expensive. Thus, it is absolutely imperative that data development and analysis efforts be consistent with rapidly evolving designs and integrity assessment methods.

In this work, we develop a constitutive description of a V–4Cr–4Ti alloy in the *unirradiated* condition for low-to-intermediate temperatures and strain rates (i.e., outside the creep and strain aging regimes). Specifically, we seek a model that accurately and compactly describes the effects of temperature (T), strain rate ($\dot{\varepsilon}$) and strain (ε) on the uniaxial flow stress, $\sigma_{\text{fl}}(T, \dot{\varepsilon}, \varepsilon)$. While not directly derived from first-principle theories, a second key objective is that the simple state variable model be physically based and consistent with the current understanding of the underlying dislocation deformation mechanisms and mechanics.

* Corresponding author. Tel.: +1-805 893 3212; fax: +1-805 893 8651.

E-mail address: donahue@engineering.ucsb.edu (E.G. Donahue).

0022-3115/00/$ - see front matter
PII: S0022-3115(00)00275-0

The research involved three steps: (a) measuring and properly reducing the requisite tensile database; (b) analyzing the general data trends in the context of simple but physically based, analytical formulations of constitutive models; and (c) quantitatively fitting the model equations to the database.

2. Experimental procedures and data reduction

Flat, dog-bone tensile specimens with a 9.0–0.5–2.0 mm long–thick–wide gauge section were prepared from a large, 500 kg heat (Heat No. 832665) of V–4Cr–4Ti manufactured by Teledyne Wah-Chang [1]. Starting at a thickness of 1.07 mm, an annealed sheet was cold rolled by collaborators at ORNL at less that 5% per pass to a final thickness of 0.5 mm with an intermediate heat treatment at 0.86 mm of 1000°C for 2 h in vacuum. Following the final cold work of about 40%, the miniature tensile specimens were punched from the sheet with their axis perpendicular to the rolling direction. The specimens were then annealed at 1000°C for 2 h in vacuum. This processing resulted in an average grain size of 25 μm and an average Vickers microhardness of 150 ± 5 [2,3].

Tensile tests were performed on a 100 kN MTS load frame with a 556 servo-hydraulic controller using a clamp-and-pin gripping system. Tests were conducted at 10 temperatures ranging from −196°C to 100°C. The desired temperatures were maintained by liquid bath (−70°C to 0°C), chilled-air baths (⩽−100°C), or by a small furnace (>20°C). Temperatures were measured by a thermocouple in contact with the specimen to within ±2°C. Strains were determined by LVDT measurements of the actuator displacement using compliance corrections provided by the slope of the elastic load-displacement curve. The tests were conducted at three nominal strain rates ($\dot{\varepsilon}$) of 4×10^{-4}, 0.04 and 2 s^{-1}. Engineering stress (s) and strain (e) were converted to their true stress (σ_{fl})–strain (ε) equivalents using the standard relations, $\sigma_{\mathrm{fl}} = s(1+e)$ and $\varepsilon = \ln(1+e)$. The yield stress (σ_{y}) was defined at the 0.2% modulus offset or, when present, at the Luder's plateau. The uniform and total engineering strains were measured at peak and fracture loads, respectively.

A total of 32 specimens were tested. Owing to the limited number of specimens, usually only one test was conducted for each condition, and not all temperature–strain rate conditions were included. Since the data were analyzed collectively, these limitations are not considered to be significant to fitting the overall constitutive model. Redundant tests showed a standard deviation in σ_{y} of about 14 MPa. Where they overlap, our results are also generally consistent with a study by Rowcliffe et al. which emphasized the regime above room temperature [4].

3. Results and analysis

Representative stress–strain curves have been reported previously [5]. Following Armstrong [6], the flow stress (σ_{fl}) is divided into yield (σ_{y}) and post-yield strain-hardening (σ_{ε}) contributions. The σ_{y} is composed of both temperature–strain rate sensitive and insensitive or, thermally activated (σ_{yt}) and athermal (σ_{ya}) components, respectively as

$$\sigma_{\mathrm{y}}(T,\dot{\varepsilon}) = \sigma_{\mathrm{yt}}(T,\dot{\varepsilon}) + \sigma_{\mathrm{ya}}. \tag{1}$$

The σ_{yt} is due to the lattice friction or Peierl's stress as well as due to small dislocation pinning points that can be bypassed with the aid of thermal fluctuations. The (low) temperature–(high) strain-rate dependence of σ_{y} in bcc metals and alloys is attributed to the low mobility of screw dislocations which experience a high resistance to slip [7]. The mechanism of screw dislocation slip is the nucleation of a kink pair; the kink segments move easily under an applied stress due to their edge character [7]. The thermally activated nucleation of kink pairs is very sensitive to temperature and stress. Thus high strain rates require correspondingly high stress and/or temperature. At a sufficiently high temperature, double kink nucleation is so rapid that the lattice friction contribution to σ_{yt} is negligible. However, thermally activated dispersed barrier strengthening by tetragonal interstitial solutes may persist at higher temperatures. The athermal σ_{ya} component is associated with hardening by polycrystalline grain structure, dislocations and larger pinning features. Note that σ_{ya} varies weakly with temperature in proportion to the elastic modulus. The development of post-yield dislocation structures results in a strain-hardening component, σ_{ε}. In fcc crystals, this contribution is relatively athermal. However, for bcc single crystals with low dislocation densities, σ_{ε} also depends on $\dot{\varepsilon}$ and T [8], suggesting a general form

$$\sigma_{\mathrm{fl}}(T,\dot{\varepsilon},\varepsilon) = \sigma_{\mathrm{yt}}(T,\dot{\varepsilon}) + \sigma_{\mathrm{ya}} + \sigma_{\varepsilon}(T,\dot{\varepsilon},\varepsilon). \tag{2}$$

3.1. Yield stress model

There is a trade-off between temperature (T) and strain rate ($\dot{\varepsilon}$) in determining $\sigma_{\mathrm{yt}}(T,\dot{\varepsilon})$: higher $\dot{\varepsilon}$ produces higher σ_{yt} corresponding to values at lower T and $\dot{\varepsilon}$. This behavior can be most simply represented in terms of a strain rate-compensated temperature (T'), defined as $\sigma_{\mathrm{y}}(T,\dot{\varepsilon}_{\mathrm{r}}) = \sigma_{\mathrm{y}}(T',\dot{\varepsilon})$, where

$$T' = T[1 + C\ \ln(\dot{\varepsilon}_{\mathrm{r}}/\dot{\varepsilon})]. \tag{3}$$

Here T is the actual absolute temperature (K) for the reference strain rate. Eq. (3) is an approximation derived from dislocation dynamics theory, where

$$\dot{\varepsilon} \propto \exp[-H'(T,\sigma)/RT] = \exp[-(H^* - V^*\sigma)/RT]. \tag{4}$$

Here $H'(T,\sigma)$ is the activation enthalpy, H^* is the activation enthalpy at 0 stress, and V^* is the activation volume. The value of $H'(T,\sigma)$ decreases with decreasing temperature and increasing stress, approaching 0 at 0 K as

$$H' = \alpha\, RT \quad \text{for } T \leqslant T_c, \tag{5}$$

where T_c is the temperature at which σ_{yt} goes to 0. For a single mechanism, C in Eq. (3) is approximately $1/\alpha$. Empirically, σ_{yt} data at different strain rates should overlap when plotted on a T' scale. The effectiveness of the T' model is illustrated in Fig. 1. Taking the slowest strain rate of 4×10^{-4} s^{-1} as the reference condition, the σ_y data at all three strain rates are plotted against T', using a 'best fit' value for $C = 0.03$. Note that the temperature shifts due to strain-rate differences are significant. For example, $\sigma_y(2\ \text{s}^{-1},\ 20°\text{C}) \approx \sigma_y(4 \times 10^{-4}\ \text{s}^{-1}, -27°\text{C})$.

The σ_y vs T' data can then be fit to an appropriate analytical expression (solid line) to provide a complete description of $\sigma_y(T,\dot{\varepsilon}) = \sigma_y(T')$. For a single underlying thermally activated mechanism an appropriate general form is [9]

$$\sigma_y(T') = \sigma_t[1 - (T'/T_c)^{1/g_1}]^{g_2} + \sigma_a(1 - \beta T), \tag{6}$$

where σ_t and σ_a are the thermal and athermal yield stress contributions at 0 K, g_1 and g_2 depend on the assumed shape of the activation barrier (typically $g_1 \approx g_2$, ranging from about 1 to 2) and β is the temperature coefficient of the elastic modulus $\approx 6 \times 10^{-5}$. As noted above, both the Peierl's stress (low temperature) and strengthening by interstitial solutes (higher temperature) contribute to σ_t. Thus, we have modified Eq. (1) to account for both processes (labeled 1 and 2) with different σ_t, T_c and g_1 and g_2. The two activated contributions are combined based on a T' weighting: as T' approaches 0, σ_t approaches $\sigma_{t12} = \sigma_{t1} + \sigma_{t2}$; as T' approaches T_{c2}, σ_t approaches σ_{t2}. In contrast to a simple summation, this formulation provides a smooth interpolation and the proper curvature in $\sigma_y(T')$ assuming $g_1 \approx g_2 \approx 1$. Thus,

$$\begin{aligned}\sigma_y(T') = {} & [\sigma_{t12} - (\sigma_{t12} - \sigma_{t2})T'/T_{c2}] \\ & \times [1 - T'/\{T_{c1} + (T_{c2} - T_{c1})T'/T_{c2}\}] \\ & + \sigma_a(1 - 6 \times 10^{-5} T).\end{aligned} \tag{7}$$

The best fit results are shown as the solid curve in Fig. 1 for: $\sigma_{t1} = 885$ MPa; $\sigma_{t2} = 125$ MPa; $T_{c1} = 170$ K and $T_{c2} = 500$ K; $\sigma_a = 245$ MPa; taking a typical value of $H(T_c) \approx 96$ kJ/mole (≈ 1 eV), the average of T_{c1} and T_{c2} (335 K) is consistent with an average $C \approx 0.03$. While the physical significance of the fit parameters should not be overemphasized, they can be broadly interpreted as crudely characterizing the two underlying activated mechanisms' slip in this alloy. The first would generally be similar in other vanadium alloys, while the second would vary with the free interstitial impurity content.

Using these values and neglecting the small effect of β, Eq. (7) can be rearranged to the convenient analytical form

$$\begin{aligned}\sigma_y(T') = {} & 1130 - 1.52T'^2 \\ & + \{(1.52T'^2 - 885T')/(170 + 0.66T')\} \quad (\text{MPa}).\end{aligned} \tag{8}$$

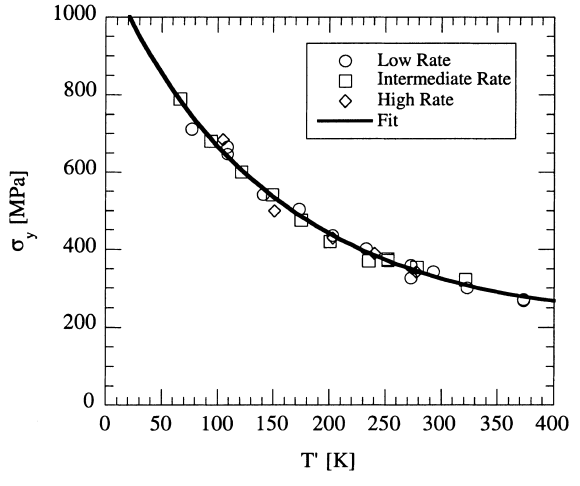

Fig. 1. Plot of σ_y vs T' for various strain rates. The two-component fit activation flow model is shown as the solid curve as described in the text.

3.2. Strain hardening

The post-yield strain-hardening contribution was experimentally defined for plastic strain levels of 0.5 to 5.0% in increments of 0.5% and from 5.0% to 14.0% in increments of 1.0% as

$$\sigma_\varepsilon(T',\varepsilon) = \sigma_{fl}(T',\varepsilon) - \sigma_y(T'). \tag{9}$$

Fig. 2 shows $\sigma_\varepsilon(\varepsilon, T')$ vs T' for the representative values of strain. The solid fit lines show slopes that are approximately zero (low ε), slightly positive (intermediate ε) and somewhat more negative (higher ε). However, on average, the slopes are approximately zero and have significant correlation coefficients only at the highest strains. The dependence of σ_ε on ε is much more significant and systematic than on T'. Thus, for a good approximation, σ_ε can be assumed to be athermal. The fcc-like *athermal* behavior of σ_ε of the V–4Cr–4Ti alloy is probably due to a high dislocation density and polycrystalline structure. The corresponding $\sigma_\varepsilon(\varepsilon)$ averaged over T' for the 19 strain levels is shown in Fig. 3. Two regimes are observed above and below an ε of about 0.025. The σ_ε vs ε data were fit to a modified Voce-type equation [10]. The Voce equation has a power law (usually linear) regime at low strains, decreasing to a

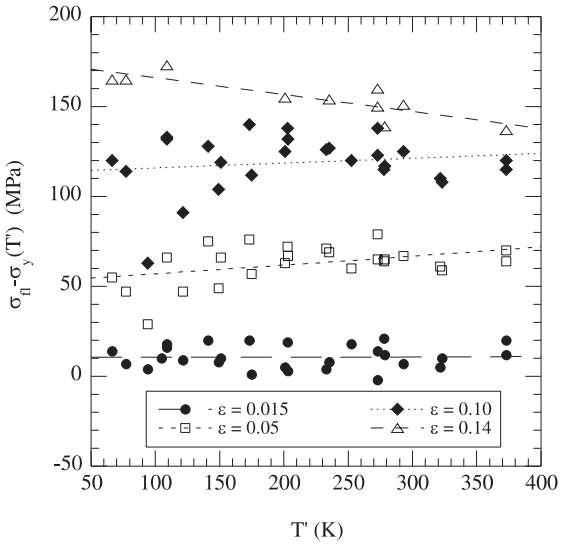

Fig. 2. Plot of $\sigma_\varepsilon(T')$ for representative strain levels, indicating a strong dependence on ε but little or no dependence on T'.

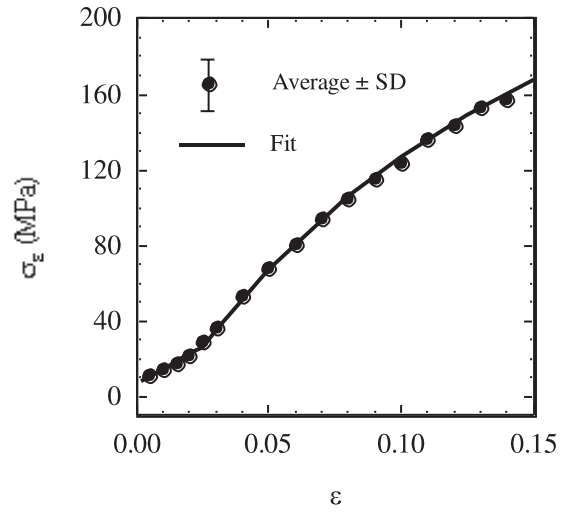

Fig. 3. Plot of σ_ε, averaged for all T', vs ε. The two-component Voce-type strain-hardening model is shown as the solid curve as described in the text.

constant saturation flow stress at higher strains. The results shown in Fig. 3 can be represented by two linear Voce-type terms with the form

$$\sigma_\varepsilon\varepsilon = \chi_{\varepsilon 1}\varepsilon[1 - \exp(-\varepsilon_{s1}/\varepsilon)] + \chi_{\varepsilon 2}(\varepsilon - \varepsilon_t \geqslant 0) \times [1 - \exp(-\varepsilon_{s2}/\varepsilon)]. \quad (10)$$

Here $\chi_{\varepsilon 1}$ and $\chi_{\varepsilon 2}$ represent the magnitude of each strain-hardening term, ε_{s1} and ε_{s2} characterize the saturation strains and ε_t is the threshold strain for the second mechanism (note $\varepsilon - 0.025$ in the second term is set to 0 for $\varepsilon < 0.025$). The solid line is the best fit given by the expression for: $\chi_{\varepsilon 1} = 865$; $\chi_{\varepsilon 2} = 1130$MPa; $\varepsilon_{s1} = 0.07$; $\varepsilon_{s2} = 0.24$; and $\varepsilon_t = 0.025$. Note, other approximate forms could be used, such as a linear term for ε between yield and 0.025 and a simple power law ($\approx 400(\varepsilon - 0.025)^{0.45}$) for $\varepsilon > 0.025$.

Eqs. (3), (8) and (10) define an overall constitutive model,

$$\begin{aligned}\sigma_{fl}(T, \dot{\varepsilon}, \varepsilon) = {} & 1130 - 1.52T' \\ & + \{(1.52T'^2 - 885T')/(170 + 0.66T')\} \\ & + 865\varepsilon\,[1 - \exp(-0.07/\varepsilon)] \\ & + 1130\,(\varepsilon - 0.025) \\ & \times [1 - \exp(-0.24/\varepsilon)] \quad (\text{MPa}). \end{aligned} \quad (11)$$

The predicted vs measured σ_{fl} at ε of 0.5, 1, 2, 4, 8 and 14% are shown in Fig. 4. The overall standard deviation of the predicted vs measured σ_{fl} is 16.4 MPa. The model can be applied over the combined T and $\dot{\varepsilon}$ ranges up to 100°C and 2/s, respectively. While some extrapolation beyond the experimental database may be reasonable, there are also limits imposed by the uniform strain regime up to about 0.14 ± 0.04.

The constitutive model can also be used to estimate the uniform strains, ε_u, in tensile tests based on the simple instability criteria that $dP/d\varepsilon \leqslant 0$, where P is the load equal to $A\sigma_{fl}$ where A is the instantaneous specimen cross-section. In the standard power law representation $\sigma_{fl}/\sigma_y = (\varepsilon/\varepsilon_y)^n$, $\varepsilon_u \approx n$. However, in the case where $\sigma_{fl} = \sigma_y + \sigma_\varepsilon(\varepsilon)$, ε_u depends on σ_y as well as the strain-hardening behavior. If σ_ε is represented in terms of a

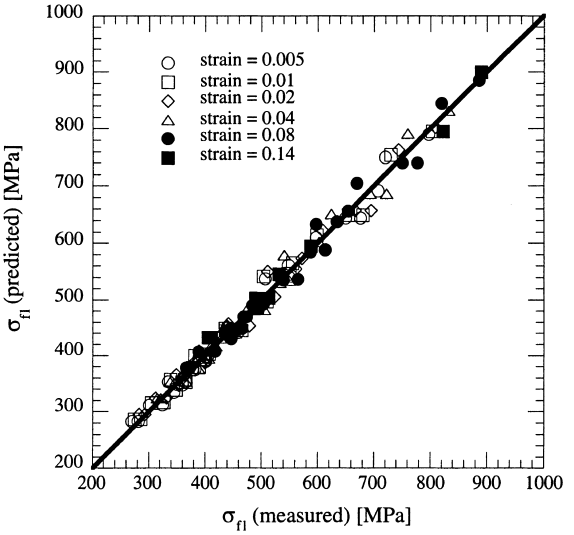

Fig. 4. Comparison of the true flow stresses measured with those predicted by the model at true strains of 0.005, 0.01, 0.02, 0.04, 0.08 and 0.14.

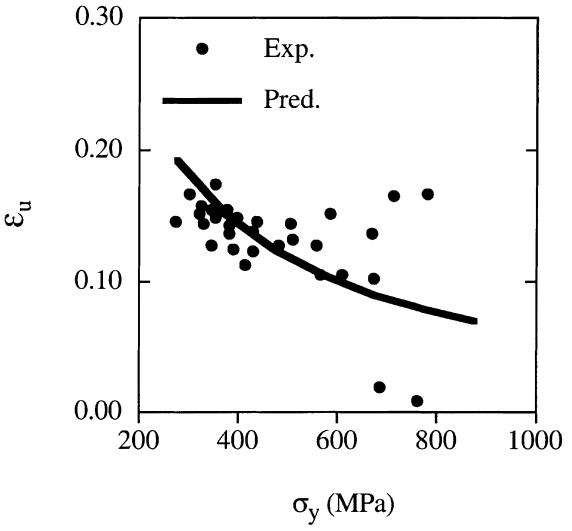

Fig. 5. Plot of ε_u vs σ_y. Predictions of ε_u are shown as solid and dashed curves as described in the text.

simple power law strain hardening $k\varepsilon^n$, ε_u (at $dP/d\varepsilon = 0$) can be found by solving the implicit relation

$$\varepsilon^{n-1} = [\sigma_y/k + \varepsilon^n]/n. \quad (12)$$

Fig. 5 compares experimentally measured values to predictions of $\varepsilon_u(\sigma_y)$ from Eq. (13) for $n = 0.45$, $k = 400$ MPa, adjusting ε and σ_y for the low-strain regime as $\varepsilon' = \varepsilon - 0.25$ and $\varepsilon'_y = \sigma_y + \sigma_\varepsilon(0.025)$. The data are in reasonable agreement with the model predictions including the trend of ε_u decreasing with increasing σ_y. Note, however, that the lowest values of ε_u are for high-rate tests that may include effects of adiabatic heating that are not included in the model.

4. Conclusions

The σ_{fl} for the program heat of V–4Cr–4Ti alloy has a classical low-temperature activated σ_{yt} regime and athermal contributions to both σ_y and σ_ε. The σ_{yt} can be represented in terms of a strain rate-compensated temperature dependence that includes contributions from both Peierl's stress and interstitial impurities. The athermal post-yield σ_ε can be described by a two-component Voce-typehardening law. The model, which incorporates analytical expressions for these processes fit to the tensile database, is broadly consistent with the current understanding of deformation in bcc alloys.

The relatively simple and compact form of the constitutive models has also a number of practical advantages. For example, it can be used to directly estimate uniform strains, as described in the previous section. In addition, FEM simulations of crack tip stress–strain fields are very sensitive to the strain-hardening behavior. If the behavior of the V–4Cr–4Ti alloy were cast in a standard Ramberg–Osgood form $[\varepsilon/\varepsilon_y \approx (\sigma/\sigma_y)^{1/n}]$, the corresponding strain-hardening exponent (n) would appear to be a strong function of T and $\dot{\varepsilon}$, since n implicitly depends on σ_y. For σ_y ranging from 250 to 800 MPa, the corresponding n varies from about 0.13 to 0.06. However, when cast in proper non-dimensional form, the predicted FEM fields are very similar over a wide range of temperatures and strain rates since: (a) σ_ε is athermal and approximately the same for various conditions; and (b) the non-dimensional fields depend only weakly on σ_y/E, where E is the elastic modulus.

Since this investigation focused on a specific vanadium alloy condition, the results cannot be directly interpreted in terms of the underlying microstructure and alloy chemistry. Developing such microstructurally based constitutive models, including the effects of irradiation and key phenomena such as flow localization, is an important objective of future research.

Acknowledgements

The authors gratefully acknowledge the assistance of J.W. Sheckherd, D. Gragg and D. Klingensmith as well as that of our collaborators, Arthur Rowcliffe and his colleagues at ORNL. The work was supported by the US Department of Energy Grant # DE-FG03-87ER-52143.

References

[1] H.M. Chung, H.-C. Tsai, D.L. Smith, R. Peterson, C. Curtis, C. Wojcik, R. Kinney, DOE/ER-0313/17, US Department of Energy, 1994.
[2] M.L. Grossbeck, D.J. Alexander, J.J. Henry, W.S. Eatherly, L.T. Gibson, DOE/ER-0313/18, US Department of Energy, 1995.
[3] A.N. Gubbi, A.F. Rowcliffe, W.S. Eatherly, DOE/ER-0313/18, US Department of Energy, 1995.
[4] A.F. Rowcliffe, D.T. Hoelzer, S.J. Zinkle, DOE/ER-0313/26 US Department of Energy, 1999.
[5] G.R. Odette, E. Donahue, G.E. Lucas, J.W. Sheckherd, DOE/ER-0313/20, US Department of Energy, 1996, p. 11.
[6] F.J. Zerilli, R.W. Armstrong, J. Appl. Phys. 61 (1987) 1816.
[7] J.P. Hirth, J. Lothe, Theory of Dislocations, McGraw-Hill, New York, 1968.
[8] M. Tang, B. Devincre, L.P. Kubin, Model. Simulation Mater. Sci. Eng. 7 (1999) 893.
[9] P. Spätig, G.R. Odette, G.E. Lucas, J. Nucl. Mater. 275 (1999) 324.
[10] E. Voce, J. Inst. Met. 74 (1968) 537.